J. Fluid Mech. (1996), vol. 321, pp. 421–441

Experiments on the rise of air bubbles in clean viscous liquids

By T. MAXWORTHY[1]†, C. GNANN[2], M. KÜRTEN[2] AND F. DURST[2]

[1] Departments of Aerospace and Mechanical Engineering, University of Southern California, Los Angeles, CA 90089, USA

[2] LSTM, Friedrik-Alexander-Universität, Erlangen-Nürnberg, Erlangen, Germany

(Received 14 August 1995 and in revised form 4 April 1996)

A number of new experiments have been performed on the rise of air bubbles in clean mixtures of distilled water and pure, reagent grade, glycerine covering a range of the relevant parameter, the Morton number, $Mo = g\nu^4\rho^3/\sigma^3$, of 10^{13}. Here g is the acceleration due to gravity, ν the kinematic viscosity, ρ the density and σ the surface tension of the mixture. In these careful measurements several scaling regimes have been found that have not been discussed before in the extensive literature on the subject. The transitions between these regimes have been delineated and attempts made to discuss the dynamical processes that might be important in each of them.

1. Introduction

There are numerous industrial processes that require the addition of gases to liquids resulting in the rise of bubbles either as individuals or in an interacting cloud. In order to advance our knowledge of the momentum, heat and mass transfer occurring during bubble rise, accurate experiments are needed not only for their own sake but also as checks on the accuracy of the analytical and numerical models of these flows.

As a result, the subject of bubble rise in a viscous fluid has a long history and a huge bibliography has been generated. The standard reference work is the book of Clift, Grace & Weber (1978, referred to as CGW in what follows), which contains a listing of over 1200 contributions to the subject of the motion of bubbles, drops and particles. There is also an excellent review of the more mathematical aspects of the subject by Harper (1972). With this in mind it would seem unlikely that further work could reveal anything that is substantially new and different from these prior efforts. We believe that the present work shows that this is not the case. By using a pair of fluids that are miscible in all proportions and that allow us to cover a wide range of the relevant parameters in a consistent manner we have, in fact, uncovered some interesting new results that reveal a number of new scaling regimes which in turn suggest the importance of different dynamical interactions within each range of parameters.

The basic problem concerns the rise of a volume, V, of air in a liquid with the following properties: density, ρ, kinematic viscosity, ν, and surface tension, σ. The density and viscosity of the air in a bubble are assumed to be very small compared with the values in the exterior fluid so that the full value of the gravitational

† Author to whom correspondence should be sent.

acceleration, g, is the relevant value to use in the following dimensional analysis. The one dependent variable that is measured is the actual rise velocity, U_T, of the bubble or the corrected value in a tube of infinite diameter U_{T_∞} which we designate as U (see §2). Under these circumstances there are two independent and one dependent dimensionless parameters.

Defining the equivalent spherical diameter, d, of the bubble, as

$$d = \left(\frac{6V}{\pi}\right)^{1/3},$$

we can then extract two truely independent parameters as

the Eötvös number, $Eo, = \rho d^2 g/\sigma$ (sometimes called the Bond number),

and the Morton number, $Mo, = g\nu^4\rho^3/\sigma^3$.

The latter dimensionless quantity is particularly useful since it contains only fluid parameters and g, and hence is constant in any one experimental sequence. However it is a somewhat inconvenient parameter to use depending as it does on ν^4. Thus the numerical range typically covers thirteen decades and grossly exaggerates the effect of the viscosity variations. We suggest that a parameter like $Mo^{1/4}$, which is linear in the kinematic viscosity, is a more realistic choice and while we feel forced to use Mo in what follow, we quote the values of $Mo^{1/4}$ in table 1 for reference. On the other hand it is clear that Eo is not the only choice for an independent parameter that contains the bubble diameter. In terms of viscosity and gravity rather than surface tension and gravity it can be written:

$$\frac{Eo}{Mo^{1/3}} = d^2\left(\frac{g^2}{\nu^4}\right)^{1/3} \text{ or in terms of } \sigma \text{ and } \nu, \text{ but no gravity, as } \frac{Eo}{Mo} = \left(\frac{d\sigma}{\nu^2\rho}\right)^2.$$

The choice of a dependent dimensionless parameter is even more extensive with at least four in common use:

$$\text{Weber number, } We = \rho U^2 d/\sigma = 4\,Eo\,/3C_d,$$

$$\text{Froude number}^2, Fr^2 = U^2/gd = We\,/\,Eo,$$

$$\text{Drag coefficient, } C_d = 4gd/3U^2 = 4/3\,Fr^2,$$

$$\text{and Reynolds number, } Re = Ud/\nu \equiv We^{1/2}\left(Eo\,/\,Mo\right)^{1/4} \text{ for example.}$$

Often, in the past, these have also been used as independent parameters, for perfectly valid theoretical reasons. We follow this example only to compare with previous results and to extract some of the scaling laws that seem to be important. Whenever possible we use true independent variables.

We note, also, that a number of velocity scales can be extracted, two of which are obvious, namely

$$U_{Fr} = (gd)^{1/2} \text{ and } U_{ST} = \left(\sigma/\rho d\right)^{1/2},$$

and which are found to be critical in what follows. A third velocity scale is less obvious,

	Glycerine (% by wt)	Temperature (°C)	Surface tension (dyn cm^{-3})	Density (g cm^{-3})	Viscosity (cP)	Mo	$Mo^{1/4}$	We_c
1	0.00	35.0	69.40	0.99390	0.71500	7.710×10^{-12}	1.67×10^{-03}	2.30
2	0.00	20.0	71.68	0.99823	1.0050	2.722×10^{-11}	2.28×10^{-03}	2.30
3	1.00	20.0	71.64	1.0006	1.0320	3.024×10^{-11}	2.34×10^{-03}	2.40
4	2.00	20.0	71.60	1.0030	1.0570	3.325×10^{-11}	2.40×10^{-03}	2.40
5	4.00	20.0	71.54	1.0078	1.1500	4.650×10^{-11}	2.61×10^{-03}	2.50
6	6.00	20.0	71.46	1.0125	1.1775	5.104×10^{-11}	2.67×10^{-03}	2.40
7	10.0	20.0	71.31	1.0221	1.3200	8.034×10^{-11}	2.99×10^{-03}	2.55
8	15.0	20.0	71.14	1.0345	1.5420	1.489×10^{-10}	3.49×10^{-03}	2.50
9	20.0	20.0	70.94	1.0469	1.7750	2.605×10^{-10}	4.02×10^{-03}	2.75
10	30.0	20.0	70.33	1.0727	2.5500	1.112×10^{-09}	5.77×10^{-03}	3.05
11	40.0	20.0	69.63	1.0993	3.8400	5.749×10^{-09}	8.71×10^{-03}	3.30
12	60.0	20.0	67.82	1.1538	9.4500	2.174×10^{-07}	2.16×10^{-02}	4.20
13	80.0	20.0	65.50	1.2085	60.100	3.769×10^{-04}	1.39×10^{-01}	
14	99.8	40.0	61.53	1.2470	275.00	1.930×10^{-01}	6.63×10^{-01}	
15	99.8	30.0	62.08	1.2523	580.00	3.710	1.39	
16	99.5	20.5	62.39	1.2597	1250.0	$7.830\times10^{+01}$	2.97	

TABLE 1. Physical properties of experimental water–glycerine combinations.

that is, $U_V = d^2g/\nu = U_{Fr}^2/U_v$, which appears rather than the more commonly used viscous velocity scale, $U_v = \nu/d$.

In §2 the details of the experimental apparatus and procedure are presented. Section 3 contains a presentation of the results conveniently divided into two sections: the high-viscosity regime, i.e. values of $Mo \gtrsim 0.19$, and the low-viscosity regimes, i.e. $Mo \lesssim 2.17 \times 10^{-7}$, while one case at $Mo = 3.8 \times 10^{-4}$ is considered to have an intermediate behaviour and is included in both. The conclusion and discussion are contained in §4.

2. Apparatus and procedure

The experiments were carried out in a cylindrical Lucite tank of inside diameter 10.2 cm and length 152.2 cm. This was filled with a mixture of triply distilled water and pure reagent-grade glycerine in various proportions (see table 1). The cylinder was surrounded by a square tank 16.6 cm on a side and the space between the two tanks was continuously replenished with water from a constant-temperature bath. We were able to maintain the temperature of the working fluid constant to better than ± 0.05°C in order to ensure that the properties of the fluid did not change during an experimental sequence. Air bubbles were introduced into the bottom of the inner tank by means of a specially designed adaptor into which syringes and hypodermic needles of various sizes could be inserted. Four different syringes ranging in total volume from 5 μl (5 mm^3) to 3 cm^3 were used to either inject a single bubble directly or, for the larger bubbles, to store them in a specially designed trap from which they could be released when a sufficient volume had been allowed to accumulate.

The velocity was found by timing bubble passage between two marks 110 cm apart within the region where the bubbles had attained their terminal velocity. Each experiment was repeated three times and the results were averaged.

The fluid densities were measured using a balance hydrometer while the fluid viscosities were measured using an Ostwald viscometer for the lower values and a

rotating disc viscometer for the larger values. The surface tension of each mixture was obtained from tables in Miner & Dalton (1953). Table 1 shows the conditions for each set of tests presented here and the relevant value of Mo and other parameters of interest. Note that the fluid properties were changed by changing both the percentage of glycerine and the fluid temperature. Also a number of extra tests were run for small values the glycerine percentage, between 1 and 6% ($T = 20°C$), in order to check that the purity of the glycerine was not causing a problem, as it had been in some earlier experiments that had to be discarded. Eventually this was found to have been caused by an undetected leak between the inner and outer chambers which allowed the unpurified bath water to contaminate the working mixture.

Small corrections were made for the fact that the bubble pressure changed as it rose in the tube. Also minor corrections were made for wall effects since the largest value of $\lambda = d/D$, where D is the cylinder diameter, was of the order of 0.12. Here we used the correction presented in CGW, p. 233, namely:

$$U_{T\infty} = U_T(1 - \lambda^2)^{-3/2},$$

which gives a correction of at most 2% to the measured terminal velocity (U_T). For simplicity, the subscript will be dropped and will use U as the terminal velocity in a tube of infinite diameter.

3. Results

The experiments covered such a huge range of Mo so that, for example, Re varied over six orders of magnitude, that it was deemed necessary to divide the results into two major groupings: the first, for large values of Mo and hence small values of Re and the second for the smaller values of Mo. The division is somewhat arbitrary and can best be explained after the results have been presented at which time we believe the criterion used will be obvious. For the moment we simply state, referring to table 1, that the first grouping includes the values of $Mo \geqslant 0.19$, the value $Mo = 3.8 \times 10^{-4}$ is considered to be a transitional or intermediate case and is included in both groups, while all values of $Mo \leqslant 2.17 \times 10^{-7}$ are included in the second grouping.

3.1. *Experiments at large values of* $Mo \geqslant 3.8 \times 10^{-4}$

The primary results of this section are shown in figure 1 in what might be called the classical form. This is a presentation in terms of two dependent variables, which allows comparison with the well-known theories of C_d *vs.* Re that have been part of the classical literature for many years. On each graph we show several lines. The primary one is the result of Rybczynski–Hadamard (CGW, p. 33) for an inviscid spherical bubble in a viscous liquid which together with the Oseen correction gives for $Re \ll 1$

$$C_d = \frac{16}{Re}\left(1 + \tfrac{1}{8}\,Re\right), \tag{3.1}$$

see e.g. Taylor & Acrivos (1964). The curve for the drag of a solid sphere is also shown, which in the Oseen limit is given as

$$C_d = \frac{24}{Re}\left(1 + \tfrac{3}{16}\,Re\right) \tag{3.2}$$

(CGW, p. 43). However as discussed in Maxworthy (1965) and CGW, p. 44, this result is only adequate up to $Re \approx 3$. In order to extend the curve to even higher Re we

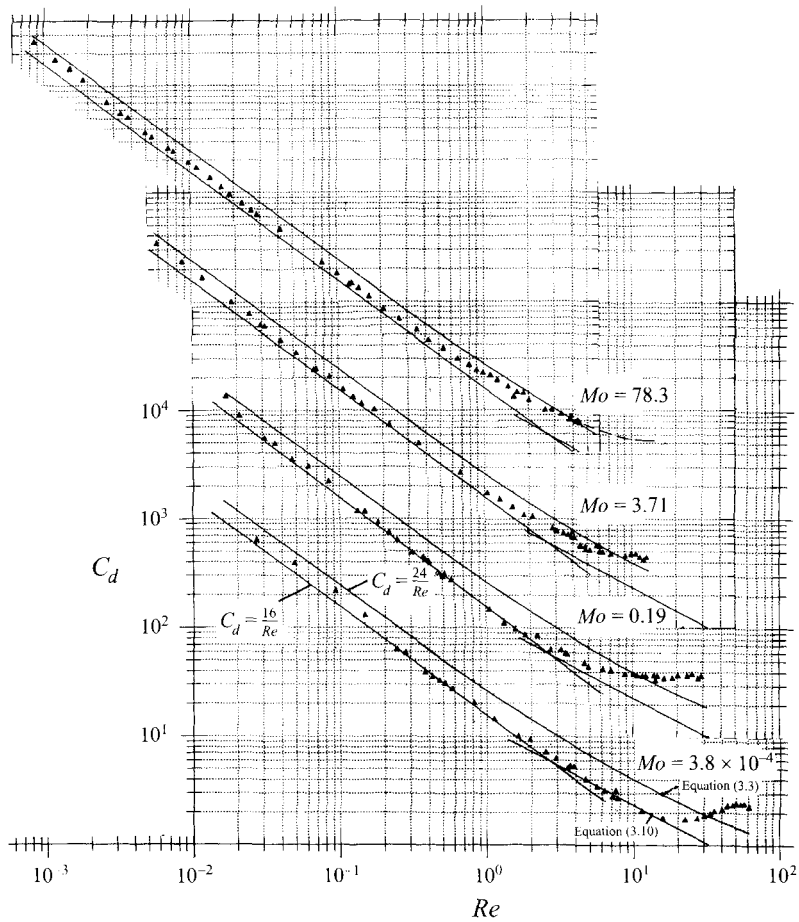

FIGURE 1. C_d *vs.* Re for the four largest values of Mo. The ordinate is correct for the lower figure and each of the curves above this is displaced vertically by one decade.

are forced to use one of the fitted curves given in CGW, p. 111. For convenience, and because it asymptotes the result above, we have chosen that due to Lapple (1951):

$$C_d = \frac{24}{Re}\left(1 + \tfrac{1}{8} Re^{0.72}\right) \tag{3.3}$$

which is accurate to +5% and −8% for $0 < Re < 1000$ (CGW, p. 111).

When we plot our results with these curves as reference (figure 1) we notice several interesting points. For the larger bubbles, i.e. the highest values of Re, the points are well above the bubble curve (equation (3.1)), and for the largest are even above the solid-sphere fitted curve (equation (3.3)), because we are dealing with bubbles that are distorted into the shape of oblate ellipsoids by the dynamical effects of the approach flow. As the bubble size (or Re) decreases further the results approach the curve for spherical bubbles, equation (3.1), and then for the smallest bubbles approach the curve for solid spheres again, (3.1) and (3.3).

We can explain part of the former effect using the results of Taylor & Acrivos (1964). In that paper they related the ellipticity (χ = major diameter of the elliptical

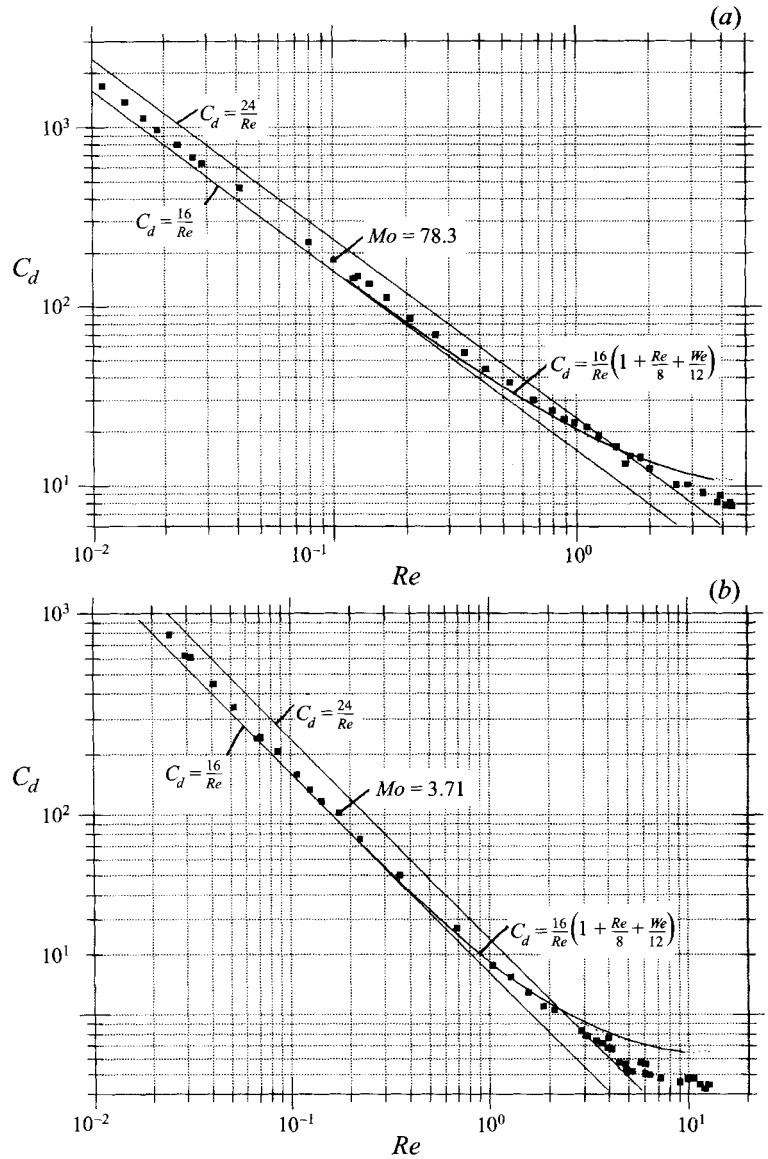

FIGURE 2. C_d *vs.* Re for (*a*) $Mo = 78.3$, (*b*) $Mo = 3.71$. Comparison with the theoretical curve of Taylor & Acrivos (1965), i.e. $C_d = 16/Re[1 + Re/8 + We/12]$.

cross-section/its minor diameter) to the Weber number as

$$\chi = 1 + \tfrac{5}{32}\, We + O(We^2), \tag{3.4}$$

and, the drag coefficient as

$$C_d = \frac{16}{Re}\left(1 + \tfrac{1}{8}\, Re + \tfrac{1}{12}\, We\right) + O\left(Re^2 \ln Re\right). \tag{3.5}$$

These results are plotted on figure 2, and a reasonable agreement found for the largest values of Mo, i.e. the smallest value of Re. Since we can write $We = Re^2\left[Mo/Eo\right]^{1/2}$ we note that the We term will dominate the Re correction when

$Mo \gg 2.25\,Eo\,Re^{-2}$. Note that this holds only for values of Re above the closest approach of the experimental points to the theoretical bubble curve. As discussed in §3.2 also, the curve for $Mo = 3.8 \times 10^{-4}$ appears to represent a transitional case between the high and low values of Mo since it approaches the lower line on the graph (i.e. equation (3.10)) which represents the limiting bubble drag curve for the lower values of Mo, as shown in §3.2.

The approach of the small-bubble drag to the solid-sphere curve for small Re needs further discussion. As pointed out in other work on this subject (e.g. CGW, p. 124) it appears that at least two effects could be important. The most likely is due to the accumulation of surface-active agents on the sphere that are then swept backward toward the rear stagnation point. This creates a surface tension gradient which generates a surface flow that opposes the primary flow around the sphere (e.g. Ogüz & Sadhal 1988). This in turn increases the drag on the sphere at these low values of We ($\chi - 1 < 10^{-5}$). Unfortunately this and similar theories could not be checked for agreement with the experiment because the amount of accumulated surface agent was unknown and could not be measured (i.e. there are two unknown quantities and only one measurement). The second effect is the hypothesized existence of a dilational surface viscosity (κ) that has a similar effect. In an attempt to quantify these effects we use the results of Agrawal & Wasan (1979), who derive the following equation for the combined effect of these two mechanisms, shown here for a bubble with zero internal viscosity, moving at low Re:

$$\frac{C_{ds}}{C_d} = \frac{3 + 4\kappa/\mu d}{2 + 4\kappa/\mu d - \frac{2}{3}F_1 d_1}, \tag{3.6}$$

where

$$F_1 = \frac{\beta \Gamma_\infty}{\mu U}, \quad d_1 = \frac{0.91 N^{1/2}}{1 + 0.53 N^{1/2}}, \quad N = \frac{4\gamma^2 U_s \mu}{dD\,(\mu + 4\kappa/3d)},$$

and μ is the dynamic viscosity of the bulk fluid, γ the coefficient of the linear relationship between surface and bulk concentration, β the coefficient of the linear relationship between surface tension and surface concentration (dyn cm g^{-1} mol), Γ_∞ the saturation surface concentration (g mol cm^{-2}), D the bulk diffusivity of surfactant (cm s^{-1}). Also $C_{ds} = 24/Re$ is the Stokes drag coefficient for a solid sphere and C_d the measured drag coefficient. In what follows we will assume initially that $U_s = d^2 g/18$, the Stokes fall velocity for a solid sphere. Two limits can be considered: the first, corresponding to $F_1 d_1 = 0$, quantifies the effect of the interfacial viscosity only, while that for $\kappa = 0$ shows the effect of the accumulation of surface-active agent. The first can be written, for $F_1 d_1 = 0$,

$$\frac{C_{ds}}{C_d} - 1 = \frac{1}{2 + (d_c/d)}, \tag{3.7}$$

where $d_c = 4\kappa/\mu$ is a critical diameter. We note for future reference that $[C_{ds}/C_d] - 1 = 1/3$ when $d/d_c = 1$. The second gives, for $\kappa = 0$,

$$\frac{C_{ds}}{C_d} - 1 = \frac{1 - \frac{1}{4}(d_c/d)^2}{2 + \frac{1}{4}(d_c/d)^2}, \tag{3.8}$$

where we have used the fact that $N \gg 1$ for typical values of the parameters and where we have set the value of $d_c = 9.1(-\beta T_\infty g\rho)^{1/2}$, so that $[C_{ds}/C_d] - 1 = 1/3$ at $d/d_c = 1$, as above. This choice of 1/3 for the critical drag ratio is somewhat arbitrary

and was chosen over what is possibly a more logical choice of 1/2 because of the fact that not all of the experimental curves touched the 'bubble-drag' line and hence this made the determination of a d_c somewhat more difficult with this value. To complete the comparison we first plotted $[C_{ds}/C_d] - 1$ *vs.* d for our data in order to determine the value of d_c. The final product is the curves shown in figure 3. Not surprisingly the trend represented by equation (3.8) seems to describe the experimental data more accurately, showing that even in this clean system sufficient impurity exists to dramatically affect the drag on the very small bubbles. The actual values of d_c found here are shown on figure 3 and plotted on figure 8, together with the values extracted from the low-Mo data using a similar technique. For the typical values of the fluid properties given in Agrawal & Wasan (1979 p. 219), we obtain a value of $d_c \approx 3.6$ mm if we use the equation for U_s quoted above. If however we use the velocity $U_s = d^2g/12\nu$, the value for a bubble in Stokes flow, d_c becomes approximately 2.9 mm. Both are close to the values found for our largest values of Mo. However, since we do not know what is contaminating our system this comparison should only be considered as a consistency argument and not as a quantitatively correct statement. The fact that the values are so close to the measured ones argues for the correctness of our identification since the value of $4\kappa/\mu$ calculated is of the order 2 cm or greater for our fluids.

3.2. *Experiments at low* $Mo \leqslant 3.8 \times 10^{-4}$

In many ways these are the most interesting of all the present results since they reveal several interesting regimes with scaling laws that have not been seen before, as far as we are aware. While what follows could be viewed basically as a curve-fitting exercise, the results obtained are sufficiently simple for us to believe that they must ultimately reveal some straightforward underlying dynamical balances. We have plotted a large number of cases in several different ways where, perhaps, only one or two were necessary to make a particular point. We have done this for two reasons: first, often the changes with the change in Mo are so subtle that we believe more than one graph is needed to show the effects and secondly we believe that these data are sufficiently basic that the maximum amount of material should be published as an archive.

We start the presentation by showing the raw data in figure 4. Noteworthy, in these curves of terminal velocity versus equivalent diameter, is the apparently universal behaviour of each curve for the larger values of d, with each curve deviating from the underlying trend by first rising above and then falling below it as d decreases, except for the largest value of Mo, i.e. the transitional curve discussed in §3.1. In order to discuss the underlying physics we need to replot the data in dimensionless form. We start with what might be called the conventional representation since the relationship between two dependent quantities, C_d and Re, is the one most often plotted. The resulting set of curves is shown in figure 5 for a number of values of Mo. As reflected in the raw data, for the large values of d, i.e. the larger values of Re for each value of Mo, the curves approach but do not reach the spherical-cap result:

$$C_d = \frac{4}{3\,Fr^2} = \frac{8}{3} \tag{3.9}$$

(CGW, p. 206) or,

$$Fr^2 = 0.5,$$

for our relatively small bubbles.

For the smallest bubbles the curves approach the solid-sphere results as seen before in §3.1 for large Mo. In between C_d goes through a very sharp minimum at essentially

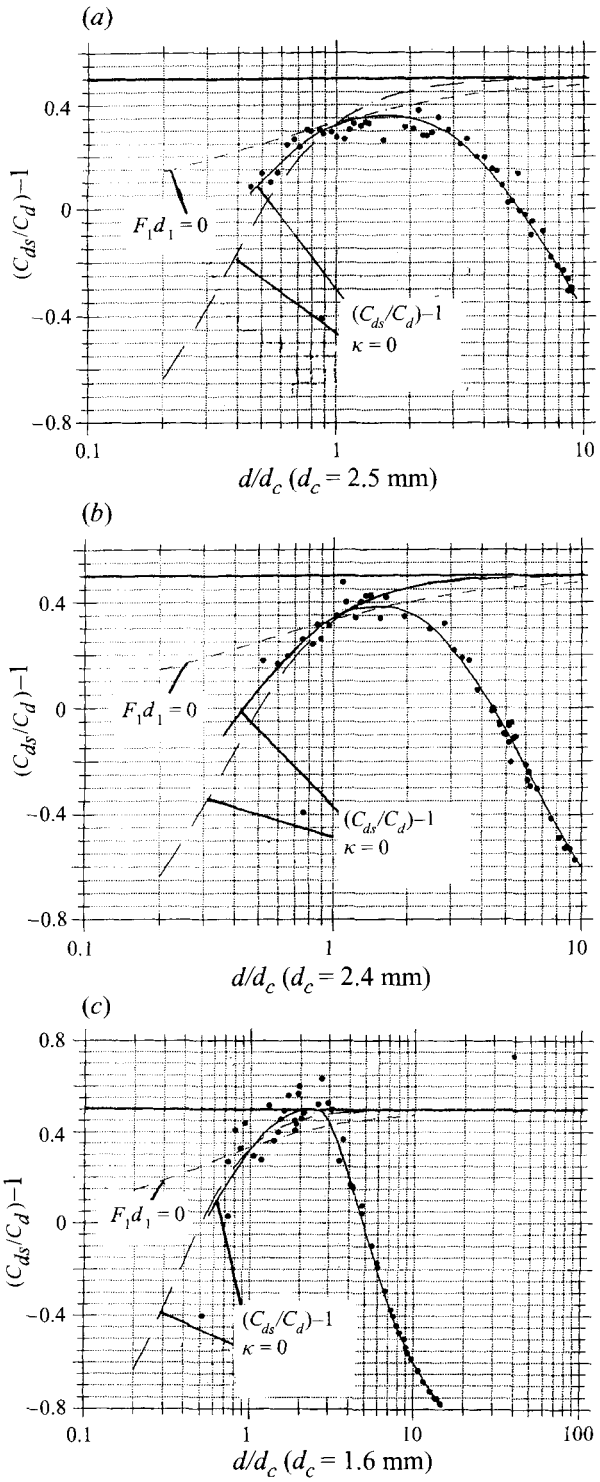

FIGURE 3. $[C_{ds}/C_d] - 1$ *vs.* d/d_c for (*a*) $Mo = 78.3$, (*b*) 3.71 and (*c*) 0.19. The theoretical curves from Agrawal & Wasan (1979) for $\kappa = 0$ and $F_1d_1 = 0$ are shown.

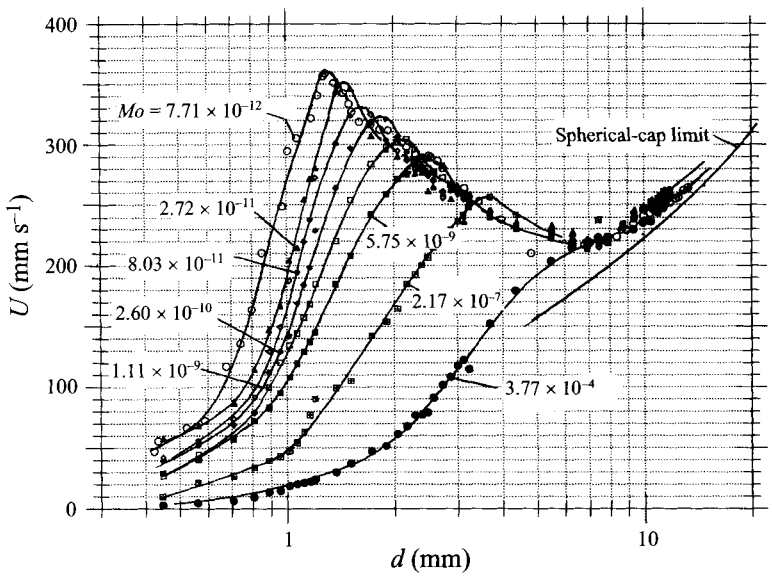

FIGURE 4. Raw data curves of U *vs.* d for selected values of Mo.

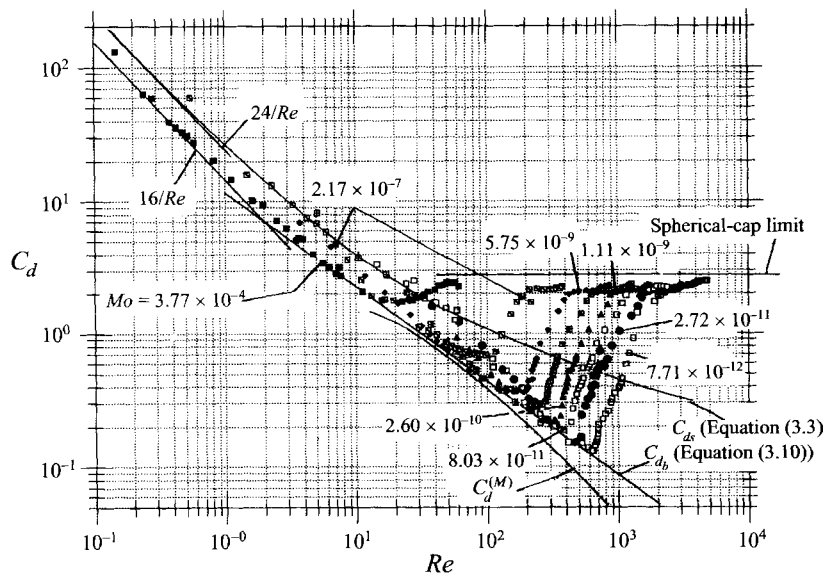

FIGURE 5. The data of figure 4 plotted as C_d *vs.* Re. The asymptotes for low-Re drag of a sphere and bubble and the spherical-cap limit are shown, as well as the C_d values for a solid sphere (C_{ds}) and the theoretical values of Moore (1963), $C_d^{(M)}$. The curve marked C_{d_b} is a straight line drawn tangentially to all of the experimental data.

the local maximum of the relevant U *vs.* d curve. This curve of transition between the two extreme cases contains a number of sub-regimes that can be anticipated by reference to figure 13, the details of which will be explained in what follows.

We note first that it is possible to draw a straight line that is closely tangent to all of the curves and which has the equation

$$C_{d_b} = 11.1\, Re^{-0.71}. \tag{3.10}$$

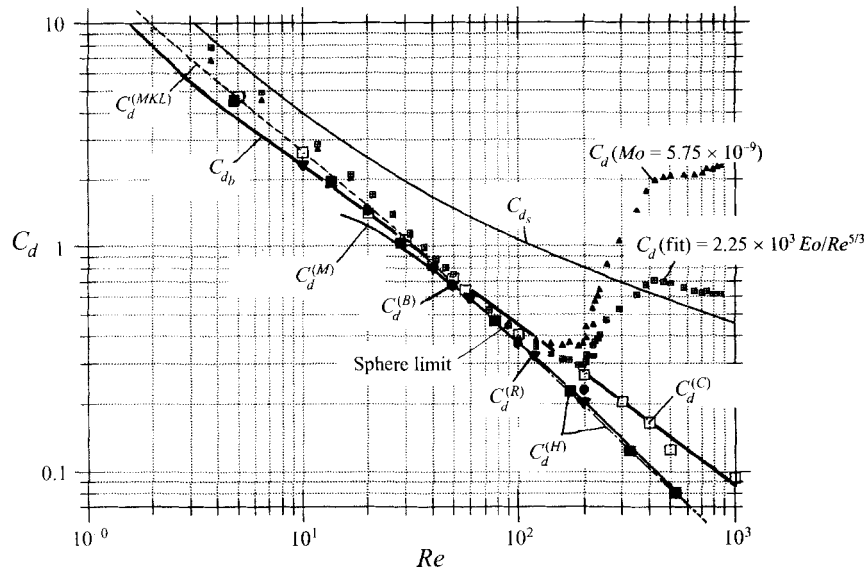

FIGURE 6. A comparison of our experimental results, C_{d_b}, with the theories of Moore (1963), $C_d^{(M)}$, Hartholdt *et al.* (1994), $C_d^{(H)}$, Ryskind & Leal (1984*a*, *b*), $C_d^{(R)}$, Brabston & Keller (1975), $C_d^{(B)}$, Mei *et al.* (1994), $C_d^{(MKL)}$, and the compilation in CGW p. 131, $C_d^{(C)}$. The curves marked C_d and C_d(fit) are the experimental values and fitted values using equation (3.13). The point marked 'sphere limit' is that at the tangent to the C_{d_b} curve and represents the bubble with the maximum eccentricity ($\chi \approx 1.1$) that reproduces the result for a sphere.

That is, at a given Re no bubble can have a drag coefficient smaller than that given by equation (3.10). We designate this as the spherical-bubble drag curve, i.e. the high-Re equivalent of the $16/Re$ line at low Re. This is to be compared to the results quoted in CGW, p. 130: $C_d = 13.7\,Re^{-0.74}$ and $C_d = 14.9\,Re^{-0.78}$. As is the case for large Mo, deviations from this curve must then be due to impurity accumulation for small bubbles and bubble distortion at high values, up to the drag minimum. To explore all of these features further we start by comparing equation (3.10) with the available analytical and numerical calculations of spherical bubble drag at high Re. These include the analytical result of Moore (1963) (designated $C_d^{(M)}$):

$$C_d^{(M)} = \frac{48}{Re}\left(1 - \frac{2.21}{Re^{1/2}}\right), \tag{3.11}$$

and the numerical results of Ryskind & Leal (1984*a*, *b*), Brabston & Keller (1975), Hartholt *et al.* (1994), and Mei, Klausner & Lawrence (1994) (their equation 2) (designated $C_d^{(R)}$, $C_d^{(B)}$, $C_d^{(H)}$, $C_d^{(MKL)}$ respectively), and of Hamielec, Johnson & Houghton (1967), Le Clair & Hamielec (1971) among many that have been combined by CGW on their p. 131. This latter curve we designate in the figure as ($C_d^{(C)}$). These comparisons are shown on figure 6 where, for the moment, experimental points marked C_d and C_d(fit), should be ignored, since they are included to demonstrate a point to be made later. We note immediately that all results are in reasonable agreement below a Reynolds number of about 100 and until the curve $C_d^{(M)}$ becomes inappropriate below a value of $Re \approx 25$. However, above $Re \approx 100$ large differences appear, with the numerical computations of Ryskind & Leal (1984*a*, *b*), Brabston & Keller (1975), Hartholt *et al.* (1994), Mei *et al.* (1994), Magnaudet *et al.* (1995) and

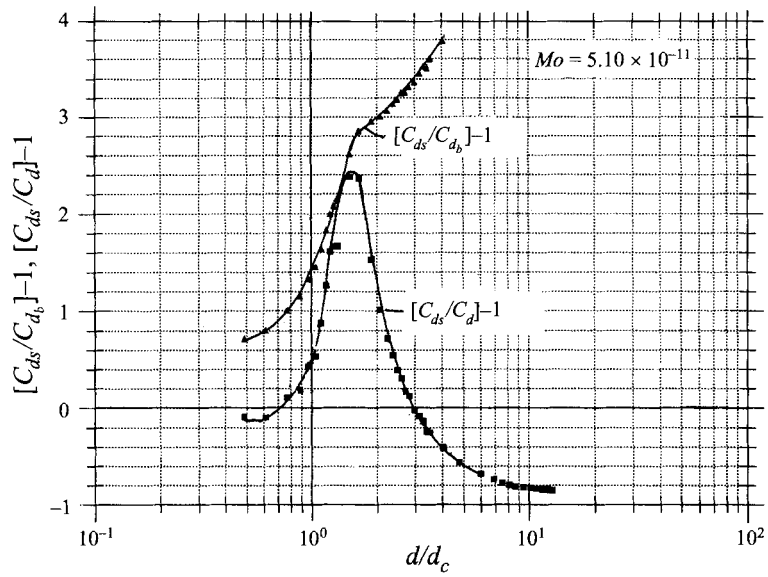

FIGURE 7. $[C_{ds}/C_{d_b}] - 1$ and $[C_{ds}/C_d] - 1$ *vs.* d/d_c showing the rapid decrease after the maximum value, as in figure 3.

Blanco & Magnaudet (1995) agreeing with Moore (1963), and those reported on p. 131 of CGW agreeing closely with our experimental line. Several points need to be discussed concerning the results. First, the surprising difference between the two sets of theoretical–numerical data must be confronted. All are for spherical bubbles in Newtonian fluids and it seems unlikely that differences in C_d of up to 100% could be due to numerical inaccuracies; and each curve is backed by four or more independent calcuations. The present authors are tempted to believe the lower curve, mainly because of its analytical basis, but each reader should to make his/her own decision on this matter based on the evidence presented here, and elsewhere in the literature, and on a detailed reading of the papers in question. Second, assuming that the limiting drag is given by lowest curve of figure 6, why are the present experimental values considerally higher at large Reynold number? Consider a typical curve of figure 5, e.g. that for $Mo = 2.72 \times 10^{-11}$. We have found that at $Re \approx 200$ the value of $We \approx 1$, so that at this stage the distortion of the bubble is already substantial ($\chi \approx 1.14$, if we use equation (3.12)) this means in turn, that the drag coefficient must be already larger that the spherical value. For smaller values of Re than this, the curve rapidly departs from the base curve (equation (3.10)) and by $Re \approx 60$ has reached the solid-sphere curve (equation (3.3)), suggesting, as shown in what follows, that even in triply distilled water the effect of impurities is important for such small bubbles ($d \leqslant 1$ mm). This all suggest that a combination of impurities and bubble distortions conspires to increase the drag above the calculated values for a spherical bubble.

Returning to the experimental data, in an attempt to quantify the effect of liquid impurities for each value of Mo we start by considering the points with values of Re below the point of tangency to equation (3.10). As in §3.1 we plot $[C_{ds}/C_{d_b}] - 1$ and $[C_{ds}/C_d] - 1$ *vs.* d/d_c where in this case C_{ds} is given by equation (3.4) and C_{d_b} by equation (3.10) and we use a technique that is the same as for the high-Mo cases but which uses the local, Reynolds-number-dependent, value of the drag coefficient

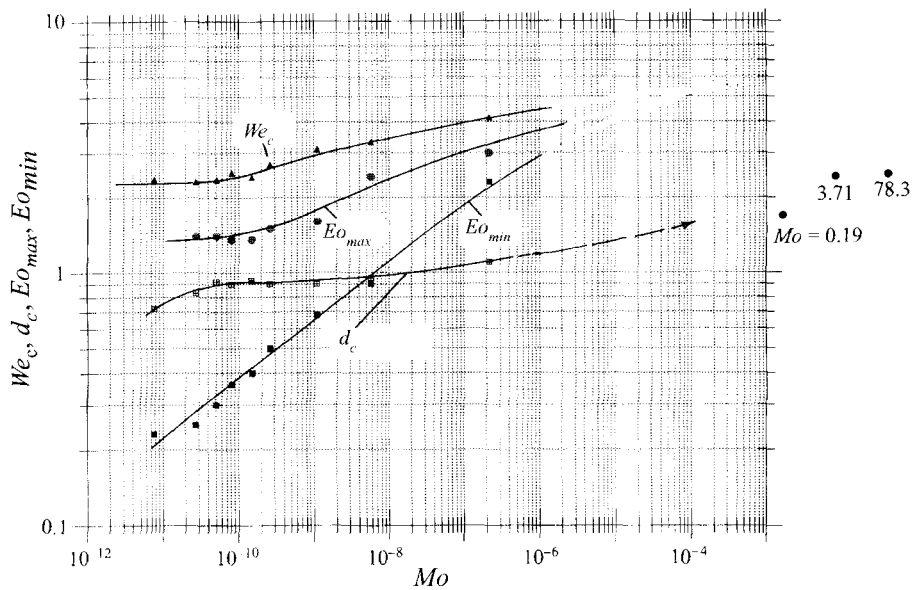

FIGURE 8. Critical values of d (d_c) taken from figures like figure 7. The value of the critical range of We (We_c) and its extent in Eo (Eo_{max}, Eo_{min}) are shown also, as taken from figures like 12 and 13.

ratio. A typical result is shown in figure 7 while a plot of d_c versus Mo is shown in figure 8. The rest of the curves on this latter figure refer to results to be discussed later. We note here that the approach to the solid-sphere curve is very abrupt, as in the case of high Mo, and again suggests, but does not prove, that the accumulation of surface-active agent is responsible for this effect.

For bubble Reynolds numbers between the tangent point to equation (3.10) and the drag minimum we have a theory to which we can refer to help explain our results. This theory, due to Moore (1965), is the high-Reynolds-numbers equivalent of the Taylor–Acrivos theory for small Re, e.g. equations (3.4) and (3.5). The bubble distortion is given in this case by

$$\chi = 1 + \frac{9}{64} We,$$

and

$$C_d = \frac{48G(\chi)}{Re}\left(1 + \frac{H(\chi)}{Re^{1/2}}\right), \tag{3.12}$$

where $G(\chi)$ and $H(\chi)$ are calculated functions that reduce to 1 and -2.21 respectively as χ tends to unity, i.e. equation (3.12) reduces to equation (3.11).

The plot of this equation for values of $Mo = 10^{-8}$, 10^{-9}, 10^{-10}, 10^{-11}, and 10^{-12} and the experimental values 2.17×10^{-7} and 5.75×10^{-9} for $We < 2$ are shown in figure 9†. Superimposed are two of our experimental curves for the latter two values of Mo with tangent points at values of $Re \lesssim 100$. One can see from this figure that the trend away from the minimum-drag tangent curve toward the minimum-drag point, for each Mo, is reproduced. However the numerical values for both cases are too high by about 30% before the drag minimum, while the trend after the minimum

† We are grateful to Professor D. W. Moore of Imperial College, London for providing us with the tables of values from which this plot and others were constructed.

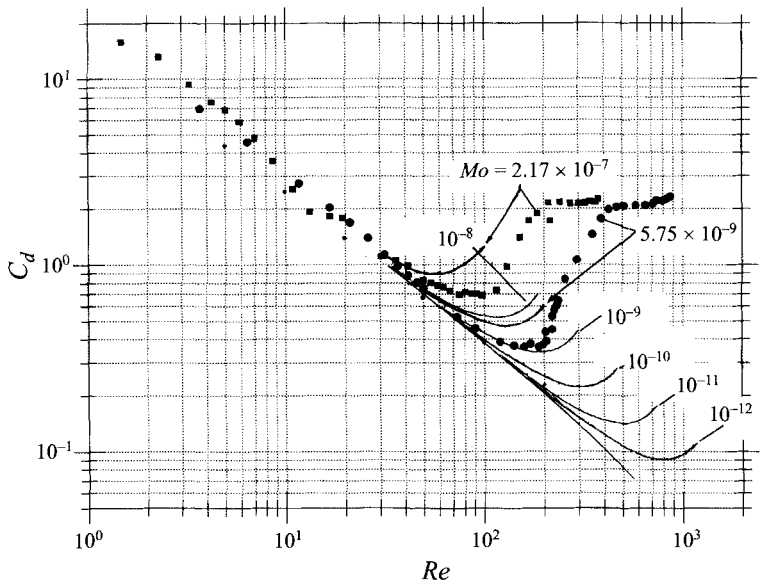

FIGURE 9. C_d *vs.* Re, for several values of Mo, from the theory of Moore (1965). Two of the theoretical curves are for values of Mo that correspond to two of the experimental values considered.

drag point is not well represented since, as we shall see, the dynamics there are quite different from those assumed in the theory. As discuss above it is likely that while the same mechanism must operate at higher values of Reynolds number, the effect is masked by the effects of very small impurity concentrations that raise the base curve (equation (3.10)) above the theoretical–numerical values. Finally we note one interesting result for the regime with Re below the minimum drag point that arose while examining the data sent to us by Professor Moore. As an exercise we plotted his values of We versus Re and noted that for all values of Mo the data below the minimum drag point followed a power law $We = h(Mo)\,Re^{1.60}$. We were sufficiently intrigued to plot our data in the same way. The result is shown in figure 10 where we see that a similar result can be found but with

$$We = f(Mo)\,Re^{5/3},$$

and

$$C_d = \frac{4}{3f(Mo)}\frac{Eo}{Re^{5/3}}. \tag{3.13}$$

By cross-plotting these data we find

$$f(Mo) = 0.526\,Mo^{0.358} \tag{3.14}$$

as shown in figure 11.

Although it is not very clear from figure 10, this power-law behaviour is followed by a region of essentially constant We and then a variation as

$$We = g(Mo)\,Re^{4/3}, \tag{3.15}$$

at least on the reduced logarithmic scale of this figure. As we will see in what follows the actual detailed behaviour is more complex than that given in equation (3.15) but

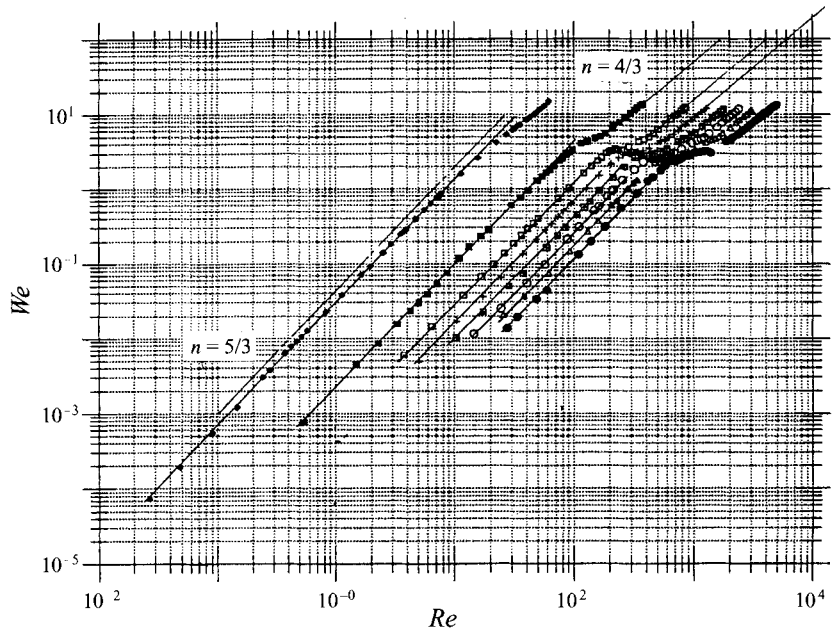

FIGURE 10. *We vs. Re* for the values of *Mo* shown in figure 5. The agreement with $We = f(Mo)\,Re^{5/3}$ below the constant-*We* region is very good as shown for one case in figure 6.

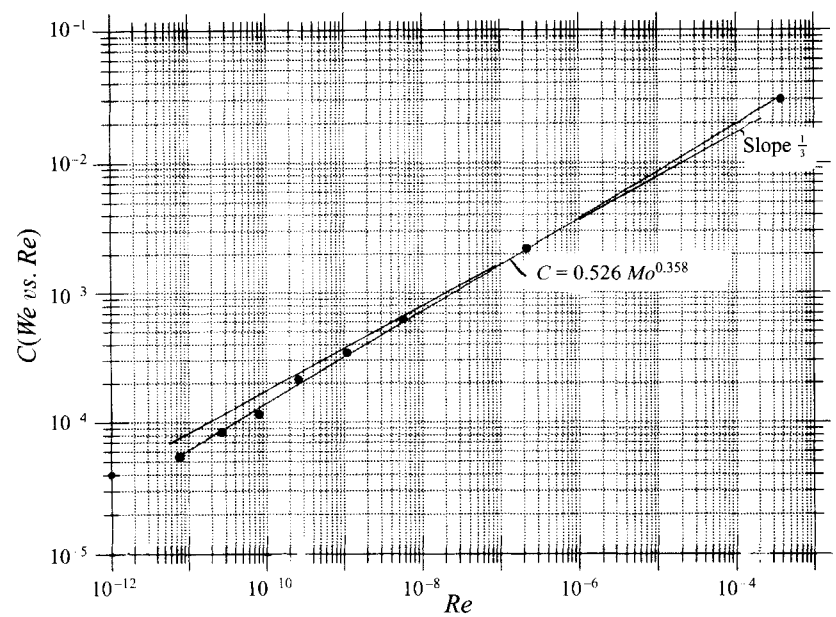

FIGURE 11. A cross-plot of the data of figure 10 to determine the function $F(Mo) = 0.526\,Mo^{0.358}$.

we believe that it is a good representation in calculations where extreme precision is not required.

Returning to equation (3.13) we show on figure 6 that it is a remarkably good approximation to the whole transition curve, both the part dominated by surface-

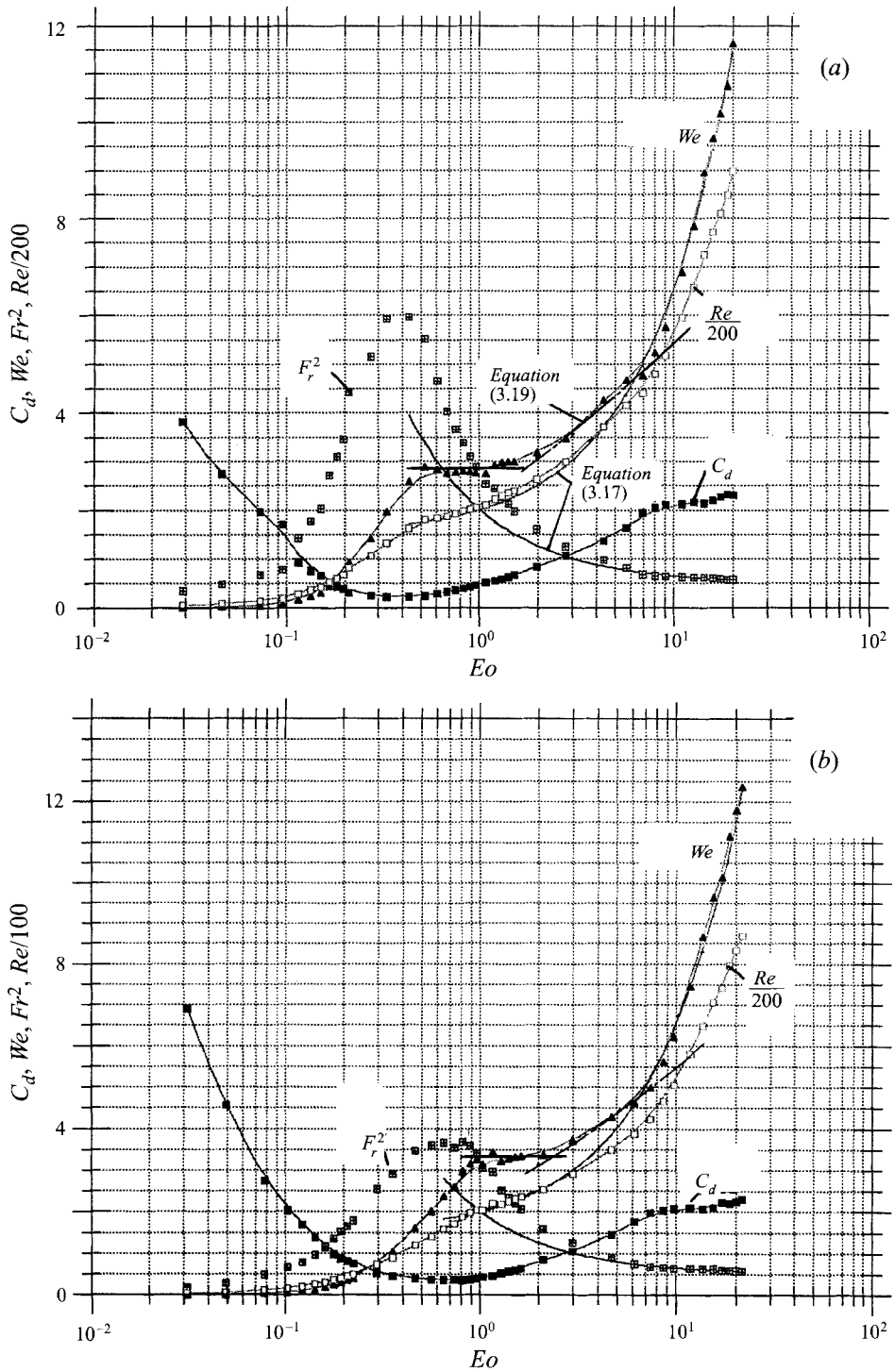

FIGURE 12 (*a,b*). For caption see facing page.

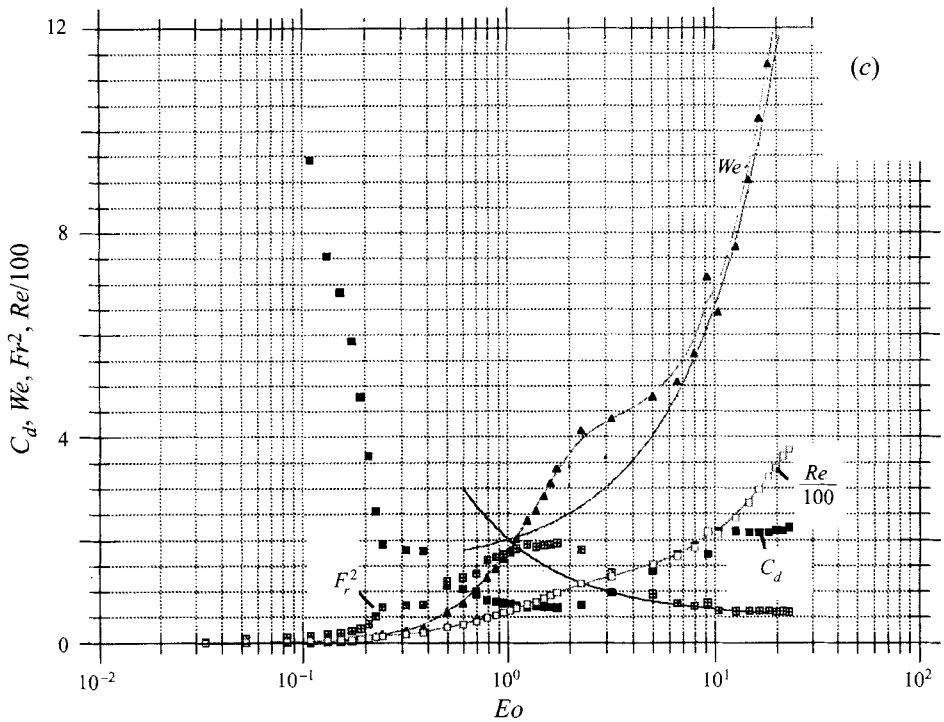

FIGURE 12. Dependent variables C_d, We, Fr^2 and Re plotted versus the independent variable Eo, for values of (*a*) $Mo = 2.605 \times 10^{-10}$ (*b*) 5.749×10^{-9} and (*c*) 2.174×10^{-7}. The regions of constant We and the asymptotes (equation (3.17)) to the spherical-cap regimes are shown on (*a*) only. Corresponding equations exist on (*b*) and (*c*), but are not included to prevent confusion.

active agents and that dominated by bubble distortion for Reynolds numbers below the drag minimum.

We can carry this curve-fitting process one step further by noting that the exponent in equation (3.14) is very close to 1/3 so that on using this fact and rearranging equation (3.13) we obtain

$$\frac{U}{d^2g/\nu} = 0.145\,Mo^{0.075} \equiv 0.145\left(\frac{g\rho^3}{\sigma^3}\right)^{0.075}\nu^{0.3}. \tag{3.16}$$

Thus in terms of the reference velocity $U_V = d^2g/\nu$ the velocity of rise is a weak function of Mo, so that for $10^{-7} > Mo > 10^{-11}$, the factor on the right-hand side varies by only a factor of 2 while U_V varies by a factor of 10 for a typical value of d. For the range of fluids of interest here the factor $(g\rho^2/\sigma^3)^{0.075}$ varies by only 7% so that to a very good degree of approximation one can ignore the variations with ρ and σ and write

$$\frac{U}{d^2g/\nu^{0.7}} \sim 0.093 \text{ in c.g.s. units and when } We \lesssim 2$$

(where we have used $\sigma = 72$ dyn cm^{-1}, $g = 981$ cm s^{-2} and $\rho = 1.00$ gm cm^{-3} in evaluating the factor $(g\rho^3/\sigma^3)^{0.075}$). It seems likely that this curve-fitting exercise has little physical significance and should not replace the explanation in terms of bubble distortion and the accumulation of surface-active agents given earlier. It should only

be used as a quick and relatively easy way to calculate the velocity of rise under the appropriate circumstances.

For values of Re, or any other variable for that matter, beyond the minimum drag point the bubble behaviour differed from that found so far. It either wobbled or followed a spiral path that grew in amplitude in proportion to the magnitude of its departure from the critical value of any particular parameter, e.g. Saffman (1956). Although the stability characteristics of the rise were observed no attempt was made to classify them except to note that unsteady bubble motion started just beyond the diameter which gave the maximum velocity of rise, i.e. the start of the constant-We regime discussed below. As the bubble size was increased even further we approached but did not reach the spherical-cap regime for our range of bubble volume. A number of approaches were tried in order to determine the scaling laws for the various dependent variables. A composite for three values of Mo is shown in figure 12, where all of the relevant dependent variables are plotted as a function of Eo. In figure 13 curves of only Fr and We versus Eo are shown for two further values of Mo but we include a designation of the various regimes to be discussed in what follows. The most revealing curves are those of We versus Eo. Beyond the location of the minimum C_d, or maximum Fr^2, We is approximately constant at a value, We_c, that varies with Mo. The approximate extent of this constant-We regime in the Eo parameter space is designated as being from Eo_{max} to Eo_{min}. The measured values of We_c, Eo_{max} and Eo_{min} are plotted on figure 8. Note that in contrast to values of We_c quoted in the published literature (e.g. Hartunian & Sears 1957) where the accuracy was not high, the present measurements are accurate to less than $\pm 5\%$ and the trends with Mo can be seen clearly.

For values of $Eo \gtrsim 7$ the approach to the spherical-cap regime can be accurately described by the relationship

$$We = 1.25 + \tfrac{1}{2} Eo. \tag{3.17}$$

Dividing by Eo, gives

$$Fr^2 = \frac{1.25}{Eo} + \frac{1}{2} \text{ or } U = \left(1.25 U_{ST}^2 + 0.5gd\right)^{1/2}, \tag{3.18}$$

so that at the usually quoted value of the transition to the spherical-cap regime of $Eo \approx 40$, $Fr^2 = 0.531$ or only slightly (6%) above the asymptotic value of 0.5. We conclude that surface tension effects slightly modified the tendency for spherical-cap behaviour in the regime $40 \gtrsim Eo \gtrsim 7$.

Finally between Eo_{max} and $Eo \approx 7$ all the curves are well approximated by

$$We = 2.5\, Eo^{1/3}, \tag{3.19}$$

as shown on the figures, or

$$U = 1.58 U_{Fr}^{1/3} U_{St}^{2/3},$$

an intimate mix of surface tension and gravitational effects, and independent of viscosity. In fact, all curves for values of Eo above Eo_{min} exhibit an independence of viscosity except that the actual value of We_{crit} depends weakly on Mo.

4. Conclusions and discussion

The conclusions are best presented by reference to figure 13 where we plot typical curves of Fr^2 and We versus Eo for values of Mo that are different from those considered in figure 12. On these we note the regimes extracted by the analysis

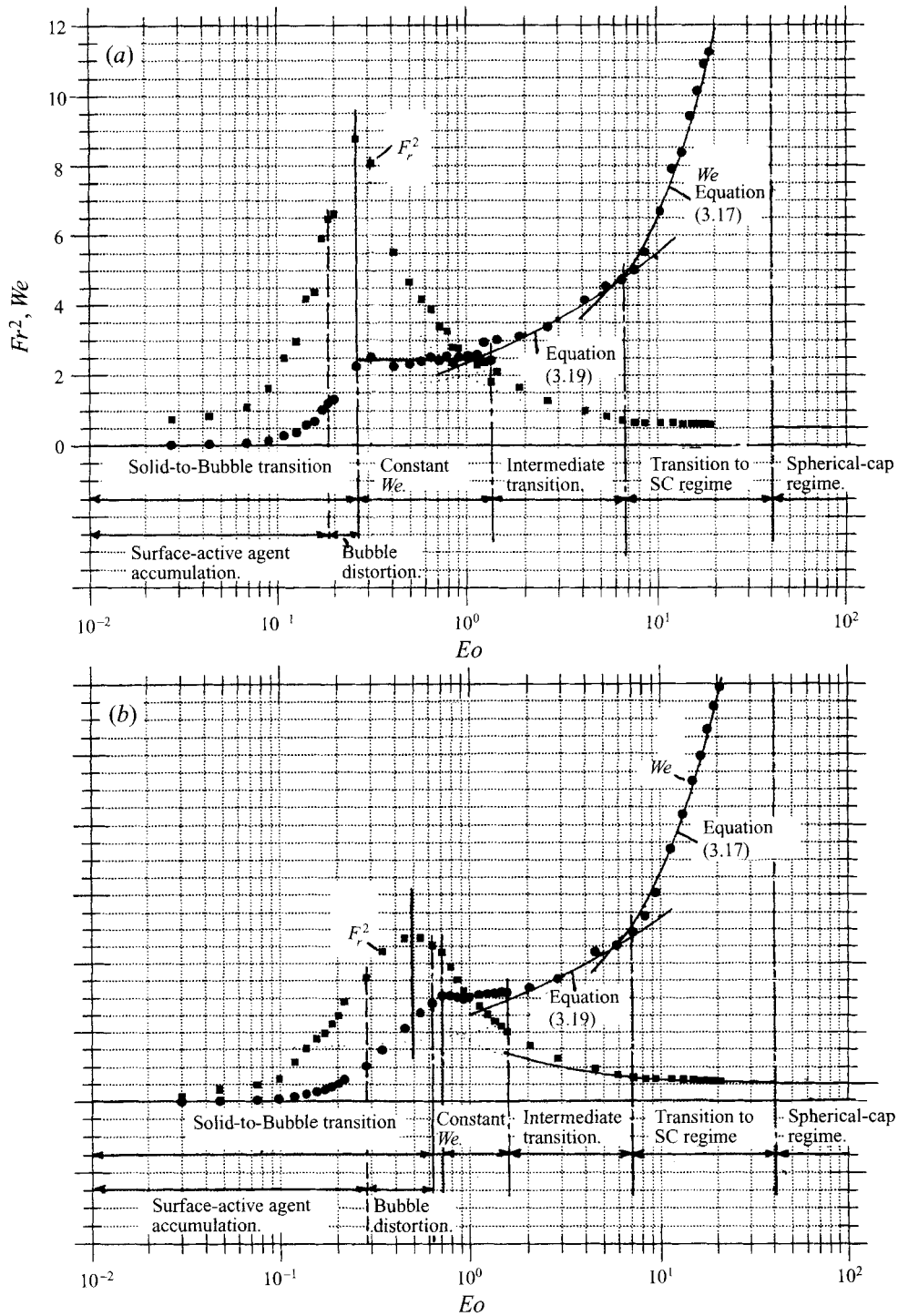

FIGURE 13. We(•) and Fr^2(■) *vs.* Eo for (*a*) $Mo = 2.722 \times 10^{-11}$ and (*b*) 1.112×10^{-9}. Here we emphasise the various sub-regimes and their transition values of Eo: (i) the solid-to-bubble transition, equation (3.13), (ii) the constant-We regimes, (iii) the intermediate or penultimate transition from We = const to ultimate transition to the spherical-cap regime (equation (3.19)), (iv) the final transition to the spherical-cap regime (equation (3.17)) (v) the spherical-cap regime (equation (3.9)).

discussed in §3.2. Surprisingly, within this very simple system we have found at least five distinct regions, or six if we include the already well-known spherical-cap regime. On these plots, the coordinates of which are independent of the fluid viscosity, the behaviour is universal beyond approximately Eo_{max} and depends only on g beyond $Eo \approx 40$. Between Eo_{min} and Eo_{max} the Weber number is constant, but at a value which depends weakly on Mo and hence on viscosity. Below Eo_{min} or alternatively the maximum of Fr^2, the results are essentially independent of the surface tension and depend only on viscosity and gravity.

These results then represent a continuous transition from a flow dominated by viscosity and gravity to one dominated by gravity alone. Between, surface tension first enters strongly in the constant-We regime and then in weaker and weaker form as the spherical-cap regime is approached, while the viscosity at first enters weakly and then not at all beyond Eo_{max}.

In view of the very distinct fractional power-laws we have found one must conclude that the underlying dynamical balances are likely to be relatively simple. For example in the region below Eo_{min} equation (3.16) suggests, to a very good approximation, that

$$U \sim \frac{d^2 g}{\nu};$$

this in turn suggests a balance between the buoyancy force and a viscous surface force, i.e.

$$\rho d^3 g \sim \left(\frac{\mu U}{d}\right) d^2$$

(where μ is the dynamic viscosity) which is essentially independent of the bubble shape and the presence of contamination below $We \approx 2$, even though we know the bubble is distorted and a small amount of contamination is present.

In the constant-We regime

$$U = \text{const.} \left(\frac{\sigma}{\rho d}\right)^{1/2}$$

a result which is independent of both ν and g except in that they determine the value of the constant. Here the balance is presumably between the dynamic pressure ρU^2 and the internal pressure σ/d which sets the bubble shape and hence the dissipation. The further transitions to the spherical-cap regime, which is itself a balance between the buoyancy force ($\rho g d^3$) and dynamic pressure force ($\rho U^2 d^2$), are more complex hybrid balances which, as far as we can see, are not yet amenable to a simple interpretation since they appear to be dominated by effects, e.g. bubble oscillation and wobble, for which no simple descriptions are possible. See however Saffman (1956) in which such an attempt is made.

The experiments discussed here were performed by C.G. and M.K., who were partially supported by internal funding at USC. T.M. and F.D. were supported in their regular faculty positions by USC and F-AU respectively.

Note added in proof: Dr J. W. M. Bush, of Cambridge University, has directed our attention to a paper by Duinivald (1995), on bubble rise in highly purified water at 19.6°C, in which he finds good agreement with the theory of Moore (1965). A careful study of his published data allows several interesting observations. Agreement with the theory occurs in the range of Re from, approximately, 150 to 300. In this range our

results are about 10–20% higher, for nominally the same value of Mo. In both experiments the minimum drag occurs at $Re \approx 510$ and the numerical values are the same to within experimental error. At lower values of Re the drag coefficients measured in his experiments rise above Moore's theory and appear to be approaching the solid-sphere drag curve also. Applying the technique used in the present paper, i.e. the one that results in figure 7, shows that, upon extrapolation, $d_c \approx 0.48$ mm and the solid-sphere drag is attained at $d \approx 0.4$ mm. This suggests that while his fluid was much cleaner than the triply distilled water used in the present experiments, even there a minute quantity of surface-active agent was present, which eventually could have accumulated on the very smallest bubbles and affected their surface boundary condition. Finally, it appears that the measured drag at the higher values of Re was unaffected and confirms that the Moore theory agrees with experiment over the range of Re quoted above.

REFERENCES

AGRAWAL, S. K. & WASAN, D. T. 1979 The effect of interfacial viscosities on the motion of drops and bubbles. *Chem. Engng J.* **18**, 215.

BLANCO, A. & MAGNANDET, J. 1995 The structure of the axisymmetric high-Reynolds number for around an ellipsoidal bubble of fixed shape. *Phys. Fluids* **7**, 1265–1274.

BRABSTON, D. C. & KELLER, H. B. 1975 Viscous flows past spherical gas bubbles. *J. Fluid Mech.* **69**, 179–189.

CLIFT, R., GRACE, J. R. & WEBER, M. E. 1978 *Bubbles, Drops and Particles.* Academic (referred to herein as CGW).

DUINIVALD, P. C. 1995 The rise velocity and shape of bubbles in pure water at high Reynolds number. *J. Fluid Mech.* **292**, 325–332.

HAMIELEC, A. E., JOHNSON, A. I. & Houghton, W. T. 1967 *AIChE J.* **13**, 220–224.

HARPER, J. F. 1972 The motion of bubbles and drops through liquids. *Adv. Appl. Mech.* **12**, 59–129.

HARTHOLDT, G. P., HOFFMAN, A. C., JANSSEN, L. P. B. M., HOOGSTRATEN, H. W. & MOES, J. H. 1994 Finite element calculations of flow past a spherical gas bubble rising on the axis of a cylindrical tube. *Z. Angew. Math. Phys.* **45**, 733–745.

HARTUNIAN, R. A. & SEARS, W. R. 1957 On the instability of small gas bubbles moving uniformly in various liquids. *J. Fluid Mech.* **3**, 27–47.

LAPPLE, C. E. 1951 *Particle Dynamics.* Engng Res. Lab., E. I. Dupont and Nemours and Co., Wilmington, Delaware.

LE CLAIR, B. P. & HAMIELEC, A. E. 1971 *Can. J. Chem. Engng* **49**, 713–720.

MAGNAUDET, J., RIVERA, M. & FABRE, J. 1995 Accelerated flows past a rigid sphere or spherical bubble. Part 1. Steady, straining flow. *J. Fluid Mech.* **284**, 97–136.

MAXWORTHY, T. 1965 Accurate measurements of sphere drag at low Reynolds numbers. *J. Fluid Mech.* **23**, 369–372.

MEI, R., KLAUSNEL, J. F. & LAWRENCE, C. J. 1994 A note on the history force on a spherical bubble at finite Reynolds number. *Phys. Fluids* **6**, 418–420.

MINER, C. S. & DALTON, N. N. 1953 *Glycerol.* Reinhold.

MOORE, D. W. 1963 The boundary layer on a spherical gas bubble. *J. Fluid Mech.* **16**, 161–176.

MOORE, D. W. 1965 The velocity of rise of distorted gas bubbles in a liquid of small viscosity. *J. Fluid Mech.* **23**, 744–766.

OGÜZ, H. N. & SADHAL, S. S. 1988 Effects of soluble and insoluble surfactants on the motion of drops. *J. Fluid Mech.* **194**, 563–579.

RYSKIND, G. & LEAL, L. G. 1984*a* Numerical solution of free-boundary problems in fluid mechanics. Part 1. The finite difference technique. *J. Fluid Mech.* **148**, 1–17.

RYSKIND, G. & LEAL, L. G. 1984*b* Numerical solution of free-boundary problems in fluid mechanics. Part 2. Buoyancy driven motion of a gas bubble through a quiescent liquid. *J. Fluid Mech.* **148**, 19–35.

SAFFMAN, D. G. 1956 On the rise of small gas bubbles in water. *J. Fluid Mech.* **1**, 249–275.

TAYLOR, J. D. & ACRIVOS, A. J. 1964 On the deformation and drag of a falling viscous drop at low Reynolds number. *J. Fluid Mech.* **18**, 466–476.